Supporting Information

Environmentally-Friendly Sunscreens: Mechanochemical Synthesis and Characterization of β-CD Inclusion Complexes of Avobenzone and Octinoxate with Improved Photostability.

Simone d'Agostino,[†] Alessandra Azzali,[†] Lucia Casali,[†] Paola Taddei,*[,‡] and Fabrizia Grepioni*[,†]

[†]Dipartimento di Chimica "Giacomo Ciamician", Università di Bologna, Via F. Selmi, 2, 40126 Bologna, Italy. fabrizia.grepioni@unibo.it

[‡]Dipartimento di Scienze Biomediche e Neuromotorie, Università di Bologna, Via Belmeloro 8/2, 40126 Bologna, Italy. paola.taddei@unibo.it

Number of pages: 28

Number of tables: 4

Number of figures: 25

Content **Page**

XRPD patterns of the reactants β-CD and avobenzone

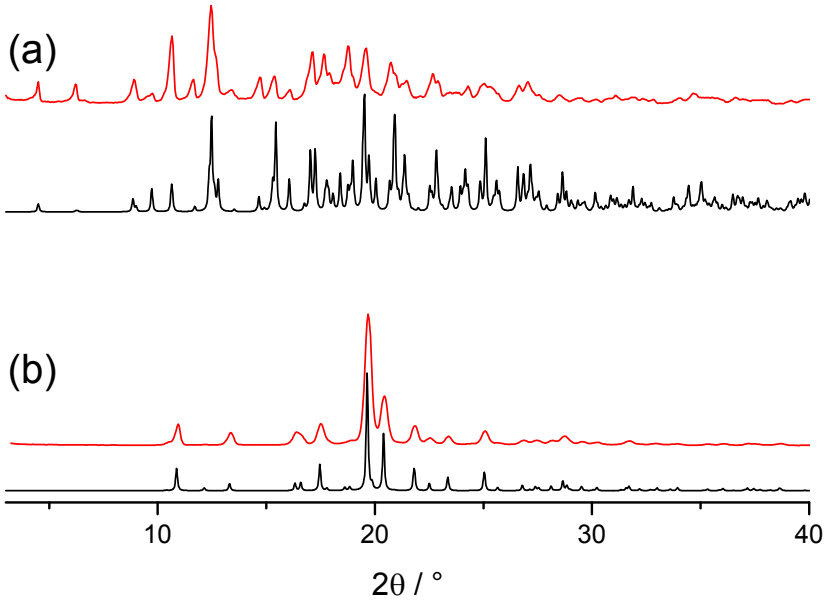

Figure SI-1. Experimental (red line) and calculated (black line) X-ray powder diffraction patterns of: (a) hydrated β-cyclodextrin (CSD refcode: BCDEXD04), and (b) avobenzone Form I (CSD refcode: WEBGAL). Polycrystalline Avobenzone Form I was obtained after recrystallization in acetonitrile.

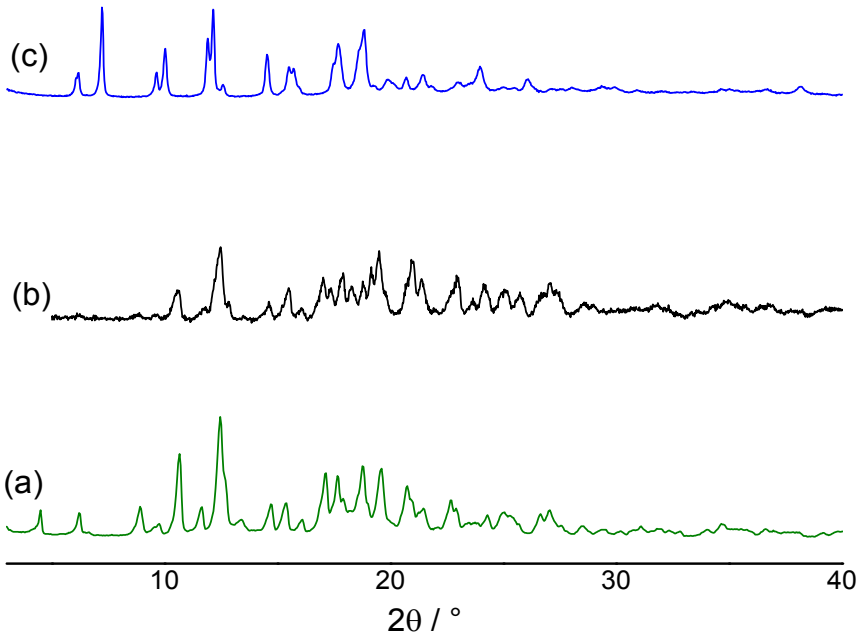

Figure SI-2. Comparison of the XRPD patterns for the mechanochemical synthesis of $(\beta\text{-CD})_3\cdot OCT_2$ from the parent materials: (a) β-CD, (b) the product obtained from grinding, and by (c) kneading with few drops of water.

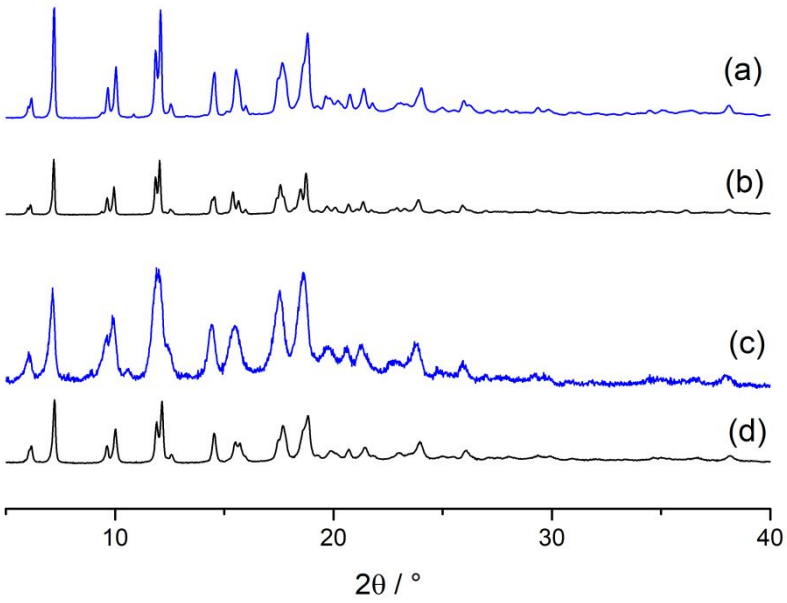

Figure SI-3. Comparison between the experimental XRPD patterns for $(\beta\text{-CD})_2\cdot$AVO obtained by kneading (a) and slurry (b), and for $(\beta\text{-CD})_3\cdot OCT_2$ obtained by kneading (c) and slurry (d).

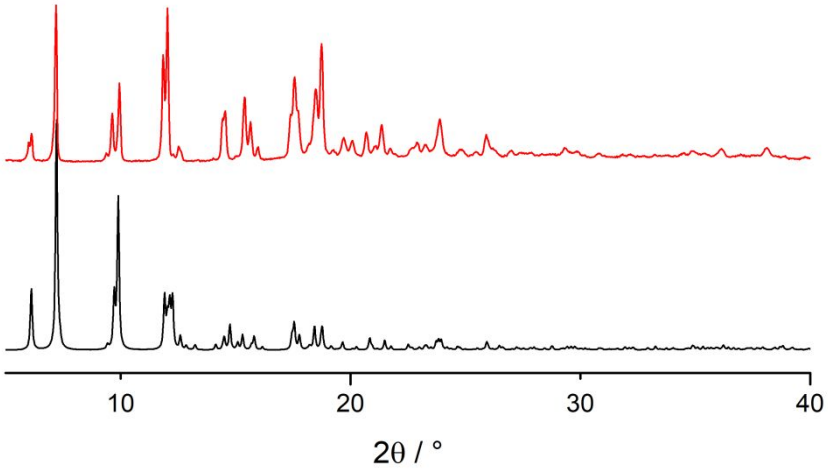

Figure SI-4. Comparison between the X-ray powder diffraction patterns of $(\beta\text{-CD})_2\cdot$AVO: (a) experimental, recorded at RT (red line), and calculated from the single crystal data as determined at 100K (black line).

Avobenzone Form II

The crystal structure of avobenzone was first published in 1993 by Kagawa et al,[1] and corresponds to the major component of commercial avobenzone. A different form was detected upon phase purity check of commercial avobenzone.

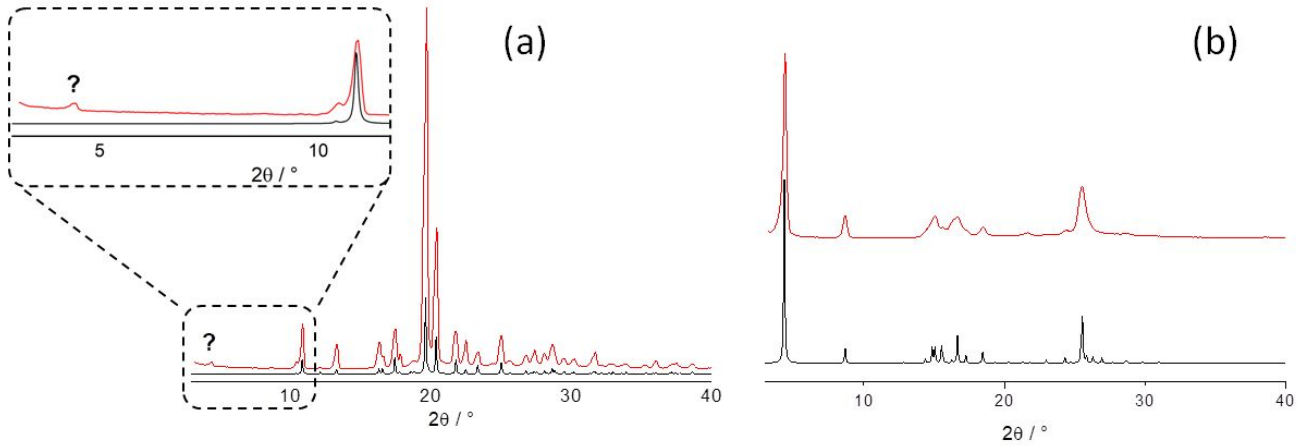

Figure SI-5. (a) The peak at low angle detected upon phase purity check of a commercial sample of avobenzone; experimental (red line) and calculated (CSD refcode: WEBGAL, black line) XRPD patterns. (b) Experimental (red line) and calculated (black line) XRPD patterns for avobenzone Form II.

Thermal analyses (TGA and DSC) allowed us to better understand the behaviour of the avobenzone polymorphic system. The TGA thermogram (Figure SI-9) of commercial powders of avobenzone, corresponding to Form I, shows a degradation process starting at ca. 150°C, while the DSC trace shows a peak at ca 87 °C (74 J/g), ascribable to the melting of avobenzone, as previously reported. The melted material was then cooled to RT and tapped with a needle. A crystallization process took place and a new DSC (Figure SI-10) was recorded. A new endothermic peak at ca 76°C (36 J/g) was detected.

Variable Temperature PXRD and Hot Stage Microscopy (Figure SI-4) were successfully applied to confirm what previously observed. Avobenzone Form I was melted at 90°C and cooled to RT to afford a high viscous amorphous material, that after tapping crystallized as polycrystalline Form II. This powder was used as seeds to grow single crystals from methanol.

In conclusion, the form obtained from melt is a new, metastable polymorph. As the new Form II is only accessible from melt, and no endothermic transition is observed in the solid state, the two forms constitute a monotropic system.

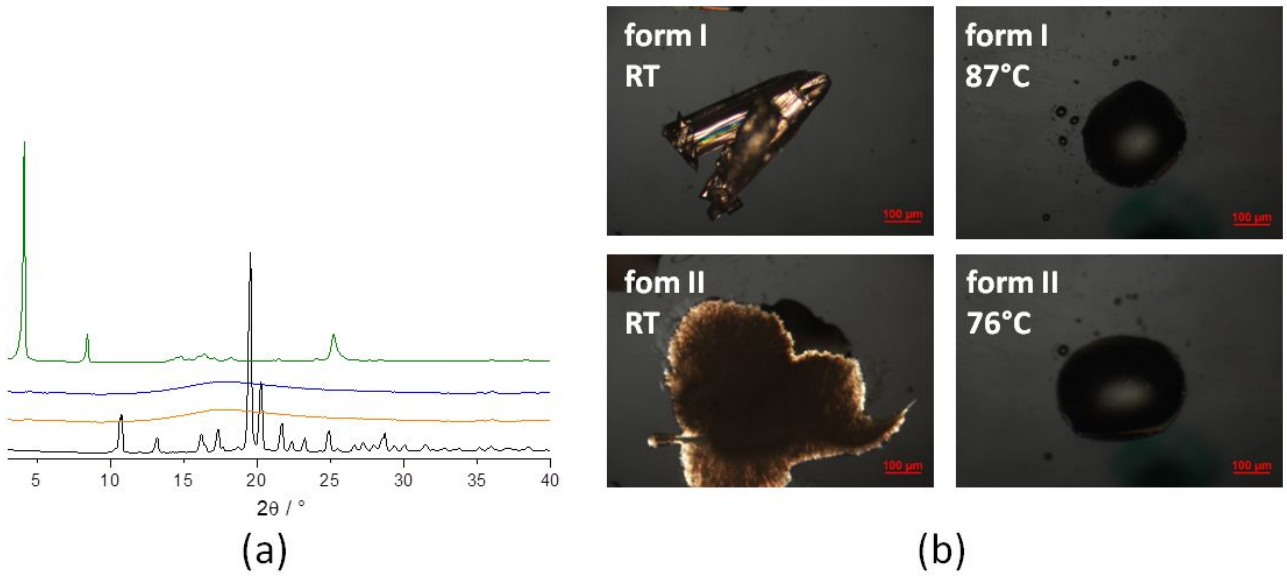

Figure SI-6. (a) VT-PXRD: avobenzone Form I (black line), melted avobenzone at 90°C (orange line), amorphous phase at RT (blue line), and avobenzone Form II (green line). (b) The same process followed by hot-stage microscopy.

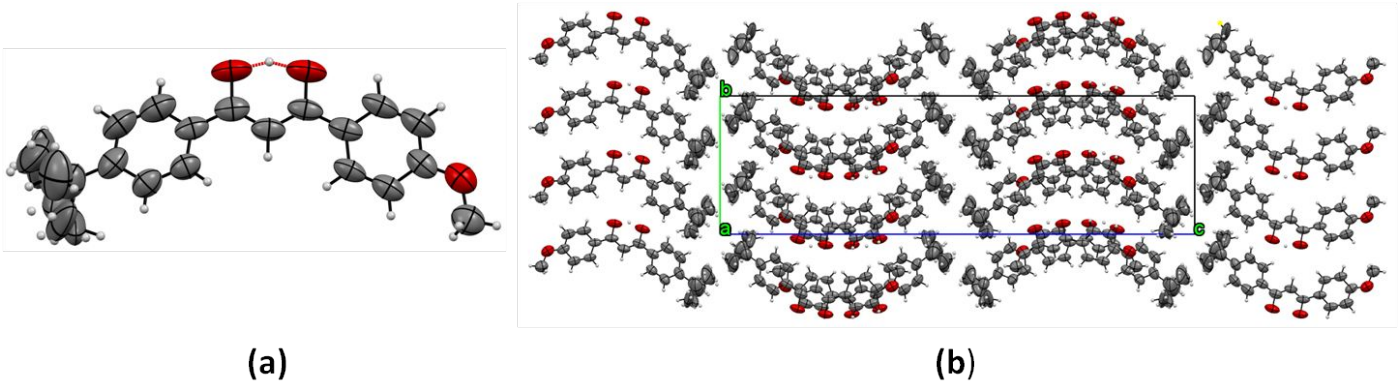

Figure SI-7. (a) Ortep Plot (thermal ellipsoids drawn at 50% probability) showing the intramolecular hydrogen bond [$O_{OH}\cdots O_{CO}$ = 2.465(6) Å] for avobenzone Form II, and (b) crystal packing viewed along the *a*-axis.

Crystal data and refinement details for crystalline avobenzone Form II and (β-CD)$_2$·AVO

Table SI-1. Crystal data and refinement details for crystalline avobenzone Form II and (β-CD)$_2$·AVO.

	Avobenzone Form II	**(β-CD)$_2$·AVO**
Formula	$C_{20}H_{22}O_3$	$C_{104}H_{178}O_{81}$
fw	310.38	2724,49
Temperature (K)	300	100
Cryst. System	Orthorhombic	Monoclinic
Space group	Pbca	C2
Z'	1	0.5
Z	8	4
a (Å)	7.3175(10)	18.9533(14)
b (Å)	11.8808(10)	24.4863(17)
c (Å)	40.778(7)	15.4504(12)
α (deg)	90	90
β (deg)	90	109.543(4)
γ (deg)	90	90
V (Å^3)	3545.1(8)	6757.4(9)
D_{calc} (g/cm^3)	1.163	1.339
μ (mm^{-1})	0.077	1.009
Measd reflns	12729	51430
Indep reflns	3124	12359
Largest diff. peak/hole (e/Å^3)	0.10/-0.09	0.46/-0.48
R_1[on F_0^2, I>2σ(I)]	0.0761	0.0650
wR_2 (all data)	0.1399	0.1925

Pawley Refinement Plots of the inclusion complexes (β-CD)$_2$·AVO and (β-CD)$_3$· OCT$_2$

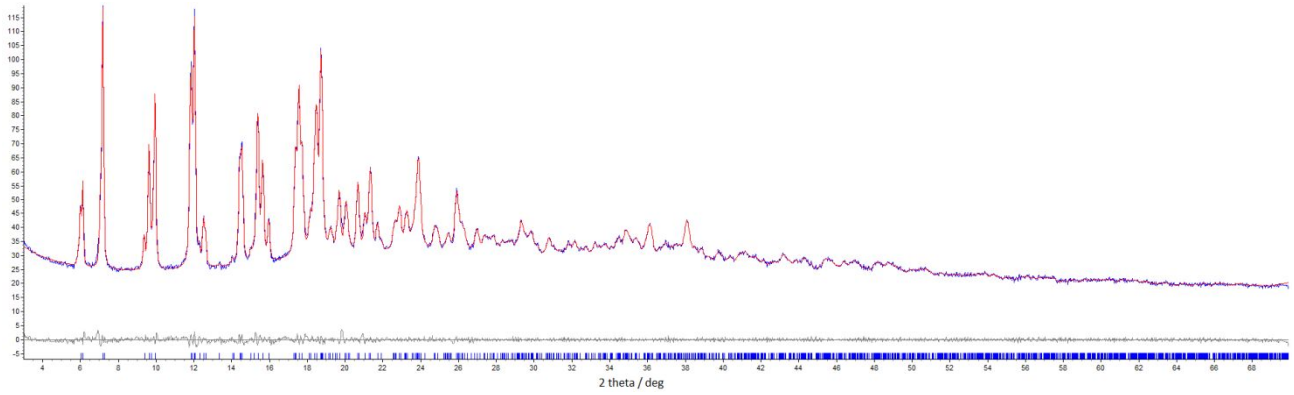

	SG	a/Å	b/Å	c/Å	α/°	β/°	γ/°	Volume/Å^3	Rwp; GoF
(β-CD)$_2$·AVO	C2	18.976(2)	24.533(2)	15.701(2)	90	110.675(8)	90	6839.6(1)	3.4%; 1.8

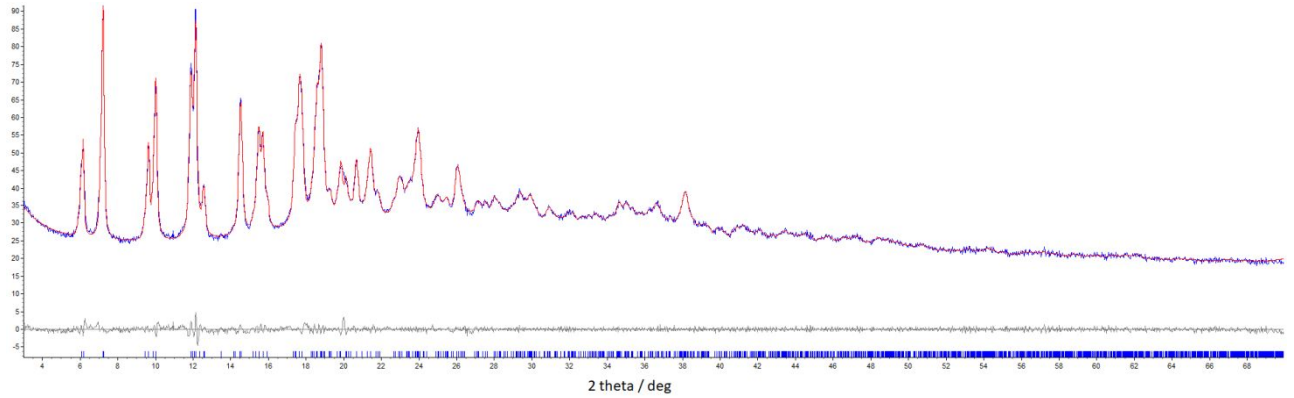

	SG	a/Å	b/Å	c/Å	α/°	β/°	γ/°	Volume/Å^3	R_{wp}; GOF
(β-CD)$_3$·OCT$_2$	C2	18.941(4)	24.433(7)	15.646(3)	90	111.39(1)	90	6742.2(9)	3.5%; 1.7

Figure SI-8. Pawley refinements plots with the corresponding unit cell parameters and FOMs for the inclusion complexes (β-CD)$_2$·AVO (top) and (β-CD)$_3$·OCT$_2$ (bottom) obtained via slurry.

^{1}H-NMR of the β-cyclodextrin (β-CD), avobenzone (AVO), and octinoxate (OCT)

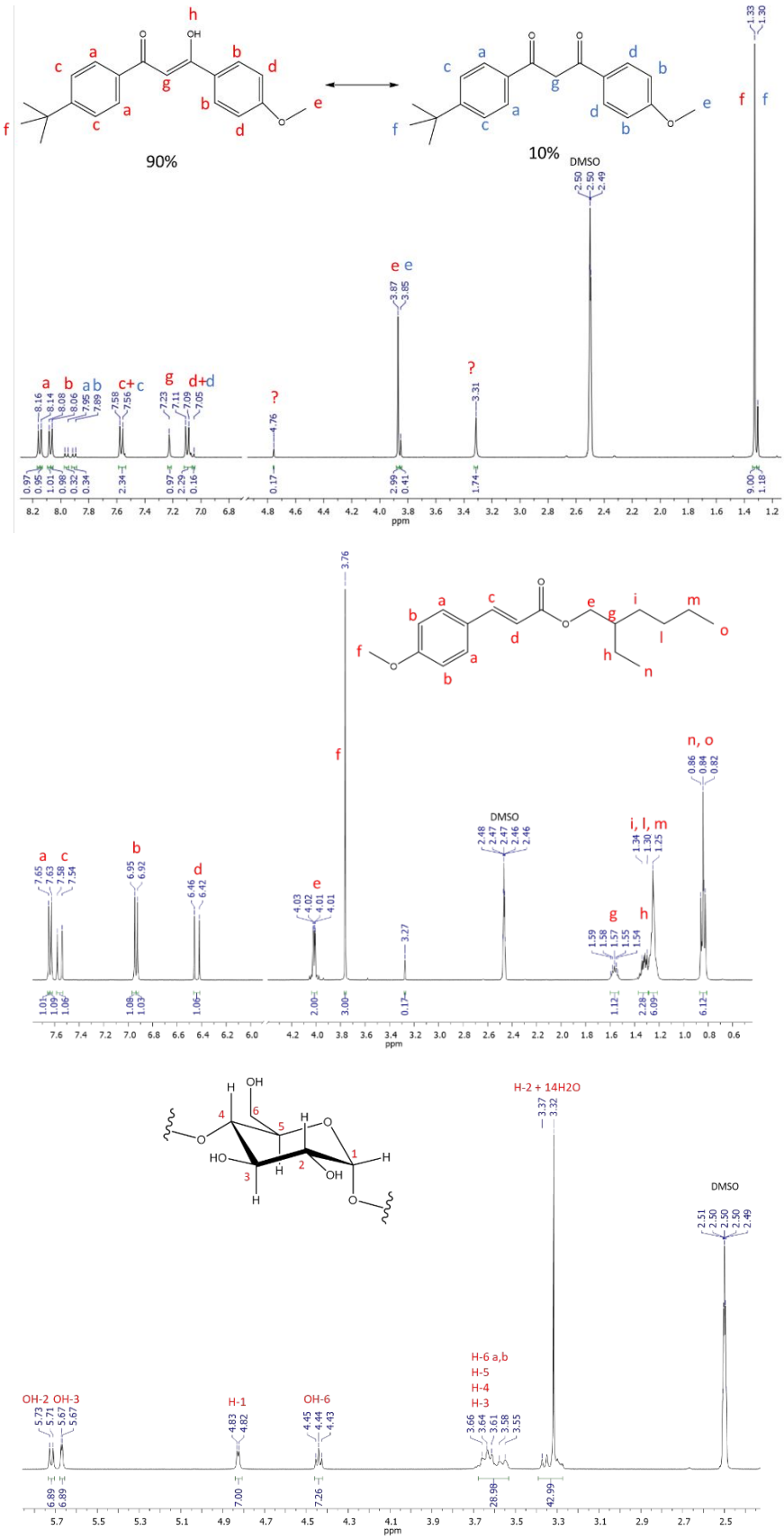

Figure SI-9. ^{1}H-NMR spectra in DMSD-d6 of the starting materials: avobenzone (top), octinoxate (middle), and β-cyclodextrin (bottom). Note: the signal assignment for the β-cyclodextrin was based on the reported one[2].

^{1}H-NMR of the inclusion complexes (β-CD)$_2$·AVO and (β-CD)$_3$·OCT$_2$

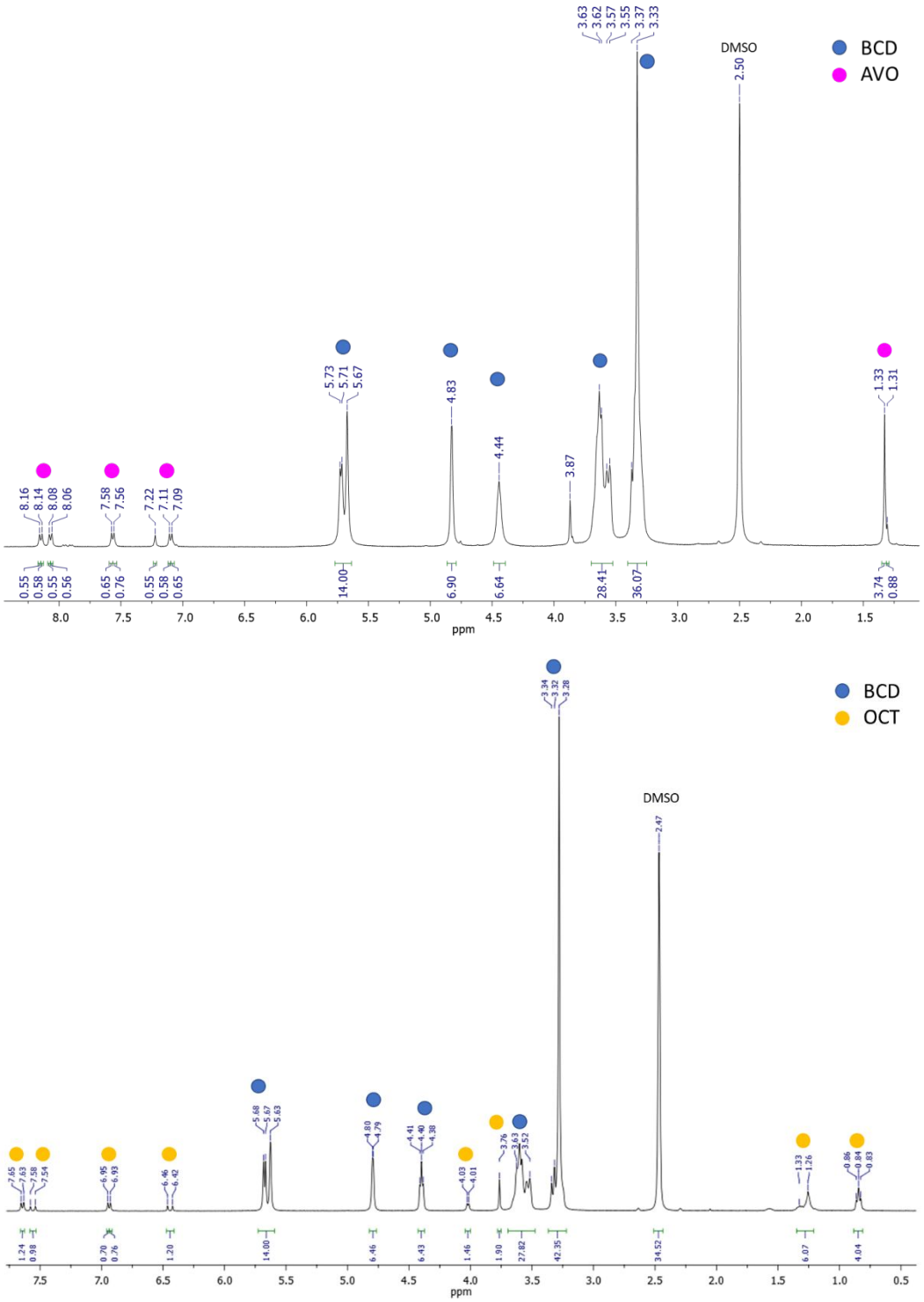

Figure SI-10. ^{1}H-NMR spectra in DMSD-d^6 of the inclusion complexes (β-CD)$_2$·AVO (top) and (β-CD)$_3$·OCT$_2$ (bottom) obtained via slurry. These ^{1}H-NMR analyses allowed to calculate the host/guest stoichiometric ratio by comparing the integration of the peaks corresponding to the two components. It must be noticed that this calculation can be done in samples containing the inclusion complex alone and the purity of these samples was verified by PXRD analysis. It results in a stoichiometry (β-CD)$_2$·AVO for avobenzone (see Figure SI-~~7~~ 10 above, peak at 8.16 ppm corresponding to one hydrogen and integrating for 0,55 H-atoms) and (β-CD)$_3$· OCT$_2$ for (see Figure SI-~~7~~10 under, peak at 7.65 ppm corresponding to two hydrogens and integrating for 1.24 H-atoms).

TGA traces

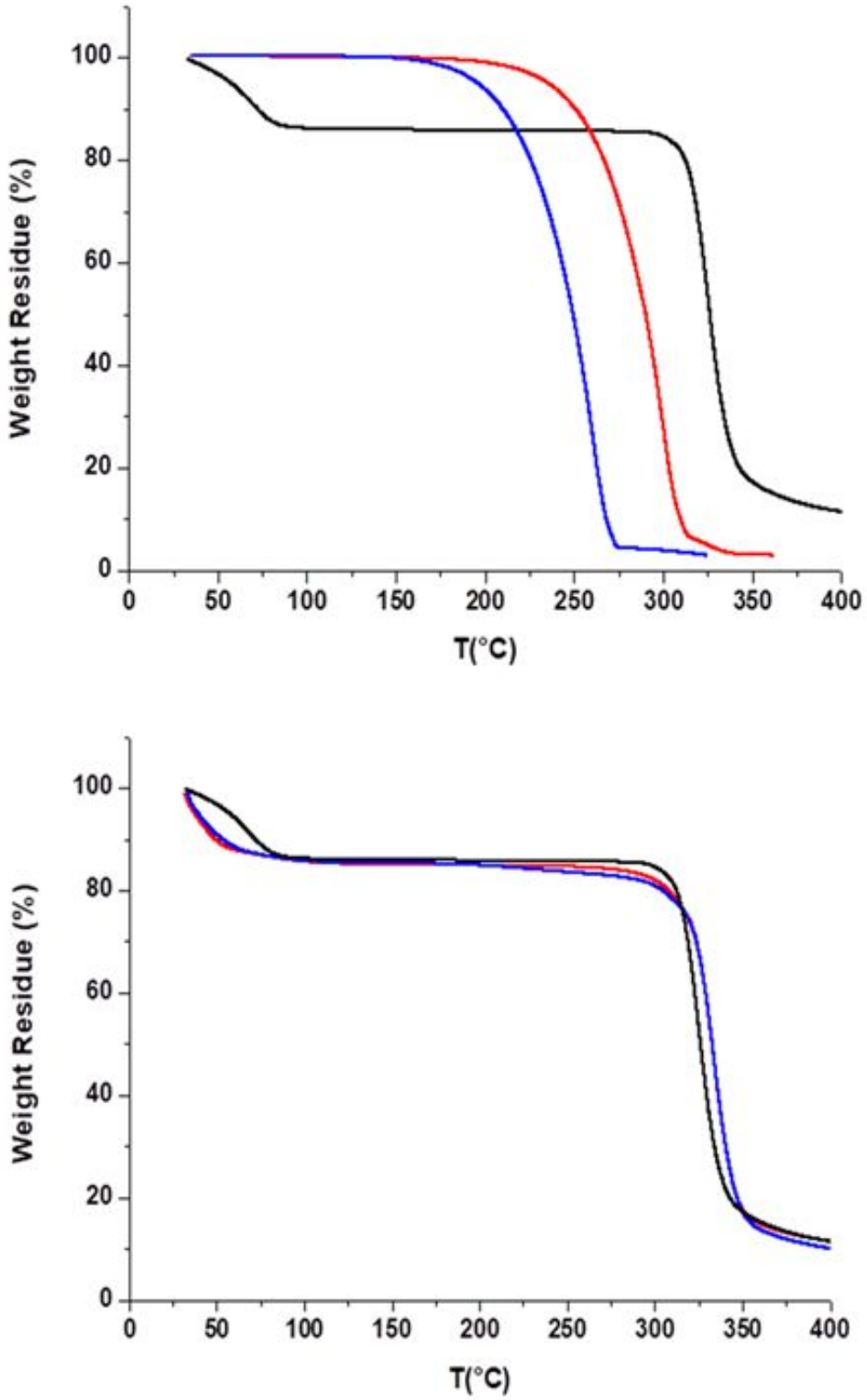

Figure SI-11. Top, TGA thermograms for β-CD (black line), avobenzone form I (red line), and octinoxate (blue line). Bottom, TGA thermograms for inclusion complexes $(\beta\text{-CD})_2$·AVO (red line) and $(\beta\text{-CD})_3$· OCT_2 (blue line) superimposed to the one of the β-CD (black line).

DSC traces

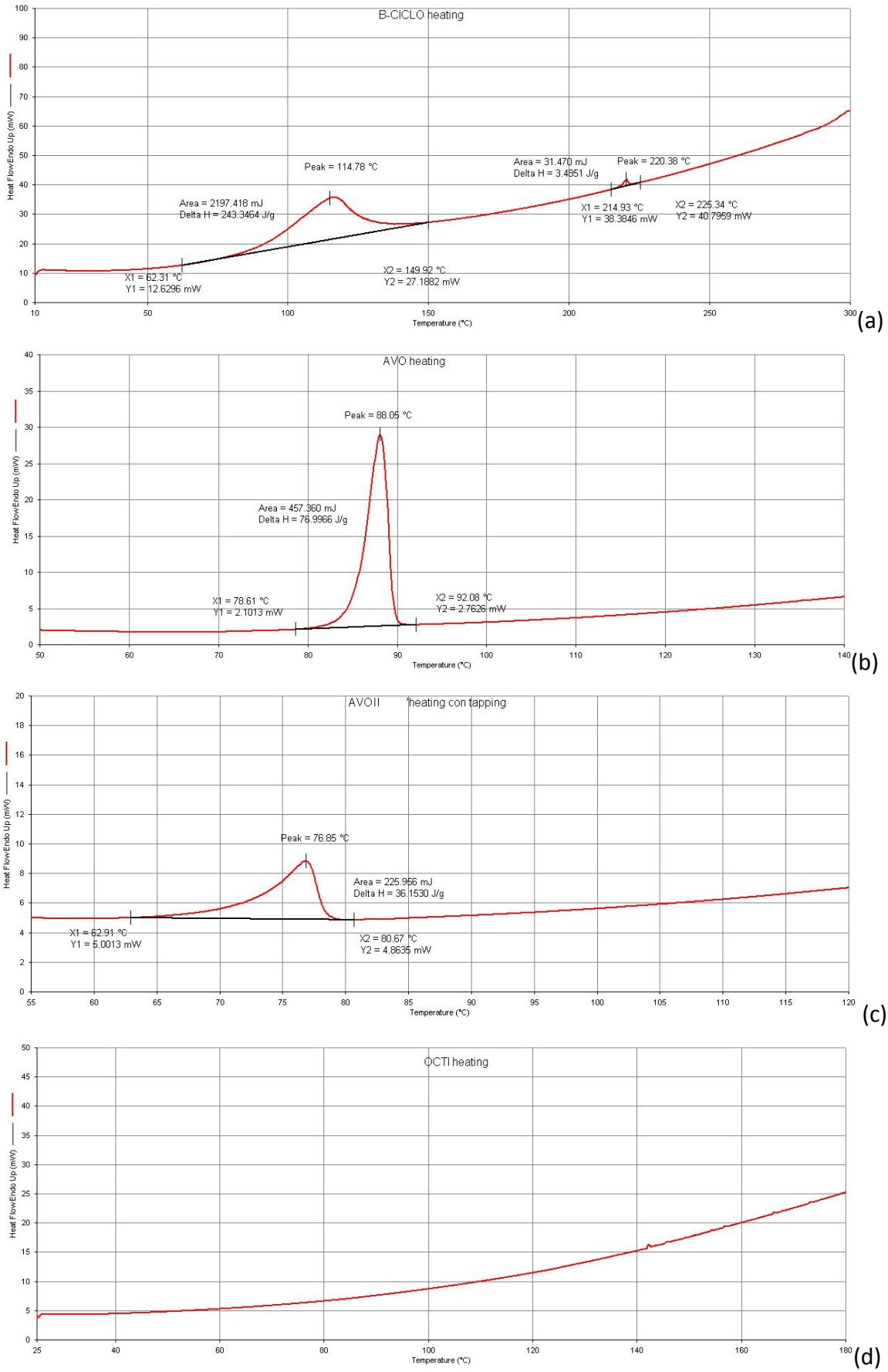

Figure SI-12. DSC traces for β-CD (a), avobenzone Form I (b), avobenzone Form II (c), and octinoxate (d).

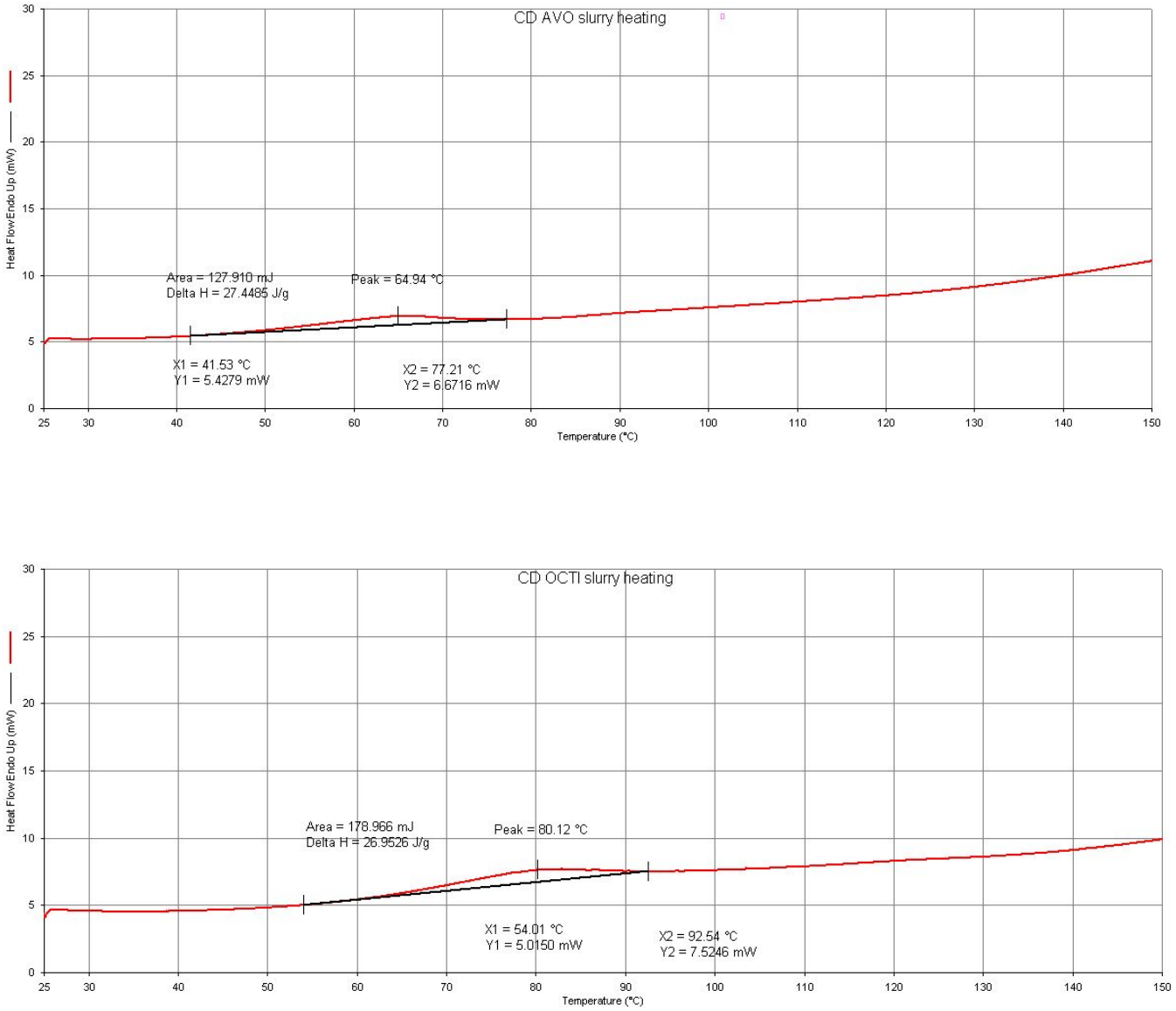

Figure SI-13. DSC traces for the inclusion complexes $(\beta\text{-CD})_2\cdot$AVO (top) and $(\beta\text{-CD})_3\cdot OCT_2$ (bottom).

Raman and FTIR spectra

Table SI-2. Raman wavenumbers and assignments[3,4] for the main bands of the $(\beta\text{-CD})_3\cdot OCT_2$ inclusion complex, octinoxate and β-CD. [For sake of clarity, octinoxate and β-CD are indicated here as O and B, respectively.]

$(\beta\text{-CD})_3\cdot OCT_2$	octinoxate	β-CD	Assignments[3,4]
~ 3290		~ 3290	OH stretching (B)
3073	3073		CH stretching (O)
2940		2937	CH stretching (B)
2903		2903	CH stretching (B)
1709	1708		C=O stretching (O)
1632	1636		exocyclic C=C stretching (O)
1604	1606		ring stretching (O)
1575	1577		ring stretching (O)
1384		1386	CH bending (B)
1327		1334	OH in plane bending (B)
1263	1267		ester and methoxy C-O stretching (O)
1253	1251		ester and methoxy C-O stretching (O)
1205	1205		methoxy C-O-C bending (O)
1170	1172		CH bending (O)
1055-1034		1049	coupled CC and CO stretching (B)
597-579		587-579	ring vibration (B)
535			ring vibration (B)
481		481	ring vibration (B)
449		441	ring vibration (B)
359		351	ring vibration (B)

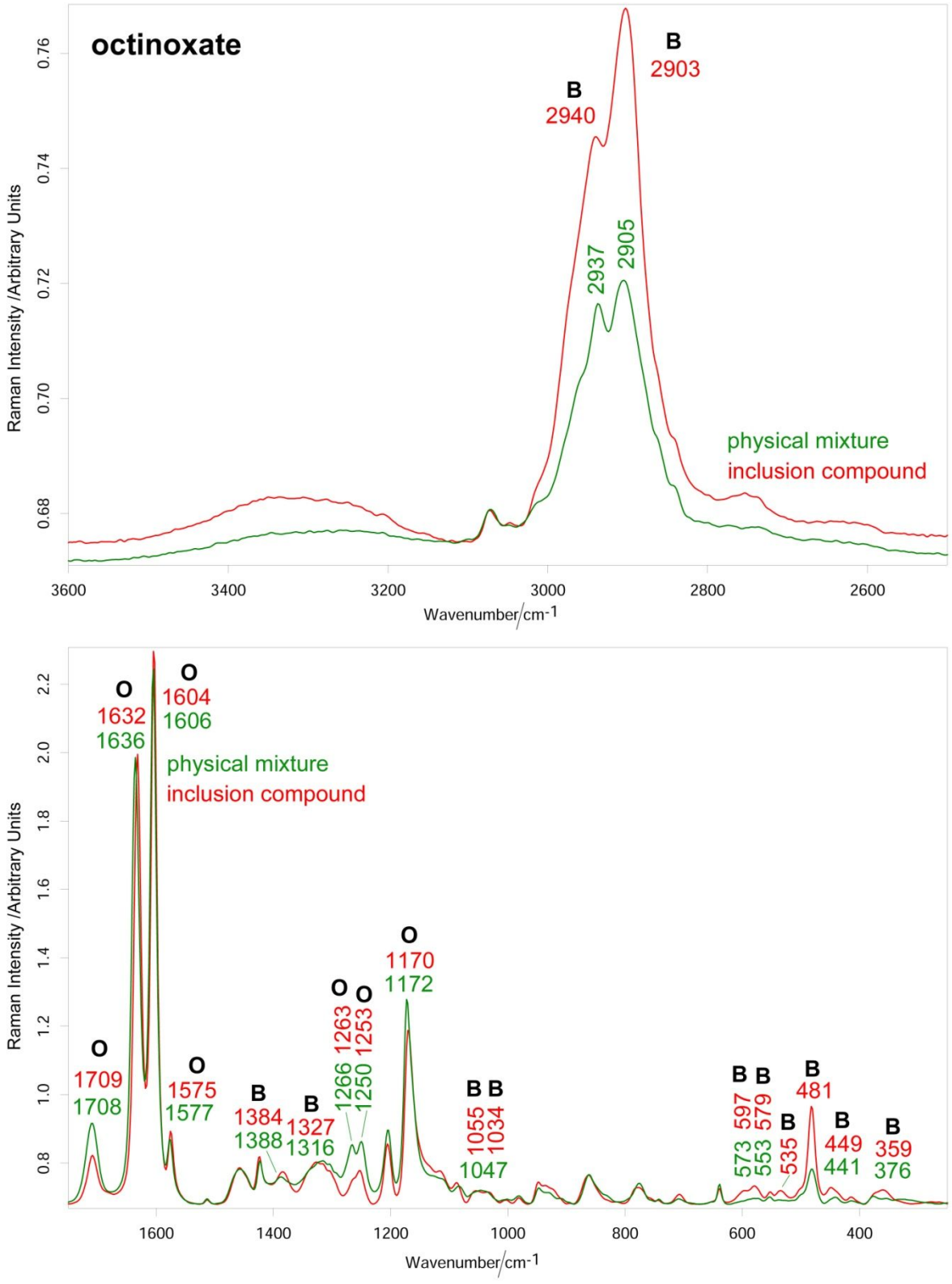

Figure SI-14. Raman spectra of the $(\beta\text{-CD})_3{\cdot}OCT_2$ inclusion compound and 3:2 physical mixture. The main bands showing differences in the two spectra are indicated, and assigned prevalently to octinoxate (O) or β-CD (B).

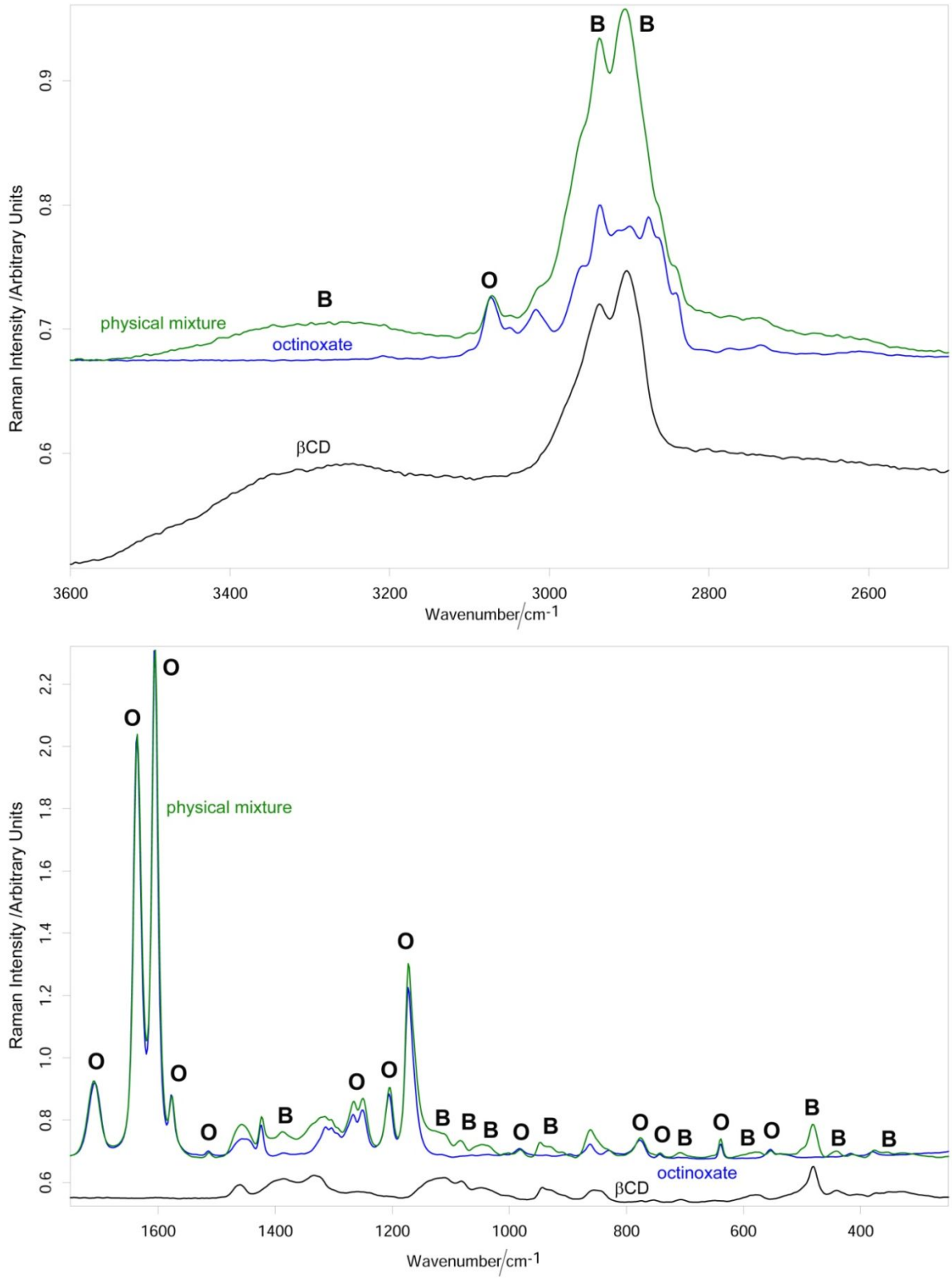

Figure SI-15. Raman spectrum of the 3:2 β-CD/octinoxate physical mixture. The spectra of octinoxate and β-CD are reported for comparison. The bands in the spectrum of the physical mixture prevalently assignable to octinoxate or β-CD are indicated with O and B, respectively. The bands not indicated have comparable contributions from both components.

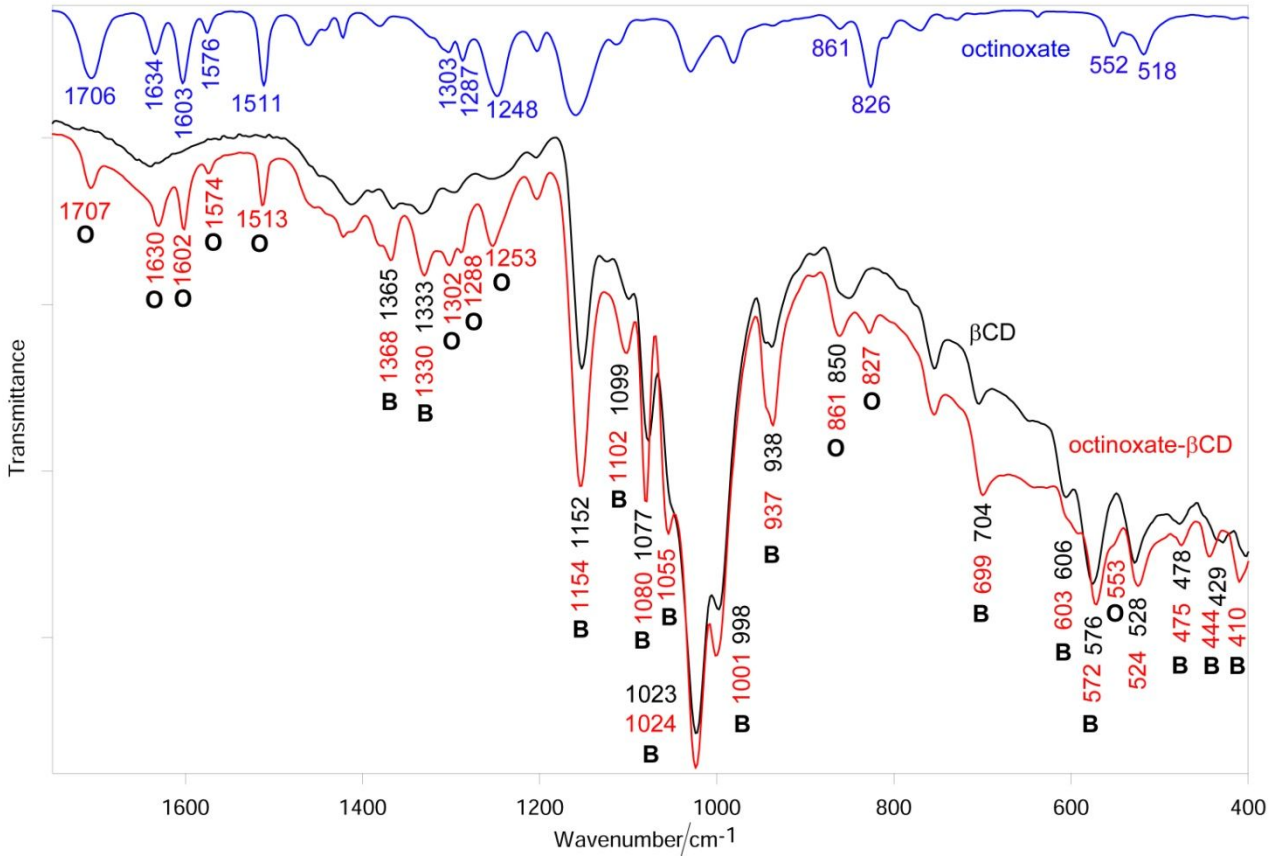

Figure SI-16. IR spectra of $(\beta\text{-CD})_3{\cdot}OCT_2$, octinoxate and β-CD. The main bands of octinoxate and β-CD that underwent changes upon formation of the inclusion compound are indicated with O and B, respectively.

Table SI-3. Raman wavenumbers and assignments[3–9] of the main bands of $(\beta\text{-CD})_2$·AVO, avobenzone and β-CD. [For sake of clarity, avobenzone and β-CD are indicated here as A and B, respectively.]

$(\beta\text{-CD})_2$·A	avobenzone form I	β-CD	Assignments[3–9]
~ 3290		~ 3290	OH stretching (B)
3074	3073		CH stretching (A)
2937		2937	CH stretching (B)
2906		2903	CH stretching (B)
1683			β-diketone C=O stretching (A)
1608	1607		C=O stretching, ring stretching coupled to C-C–C=O asymmetric stretching (A)
	1557		ring stretching coupled to C-C–C=O and OH bending (A)
1513	1518		ring stretching coupled to C-C–C=O and OH bending (A)
1383		1386	CH bending (B)
1309	1298		C-O stretching (A)
1263	1260		methoxy C-O stretching (A)
1230	1231		methoxy C-O stretching (A)
1197	1200		methoxy C-O-C bending (A)
1175	1170		CH bending (A)
1111	1114		CH bending + CO stretching (A)
1088		1082	coupled CC and CO stretching (B)
1055-1031		1049	coupled CC and CO stretching (B)

948		944	ring vibration (B)
865		856	C1 group vibration (B)
772-756	774-756		CH out-of-plane bending + ring deformation (A)
700	698		ring deformation + CH out-of-plane bending (A)
599-580		587-579	ring vibration (B)
535			ring vibration (B)
481		481	ring vibration (B)
449		441	ring vibration (B)
415		406	ring vibration (B)
357		351	ring vibration (B)

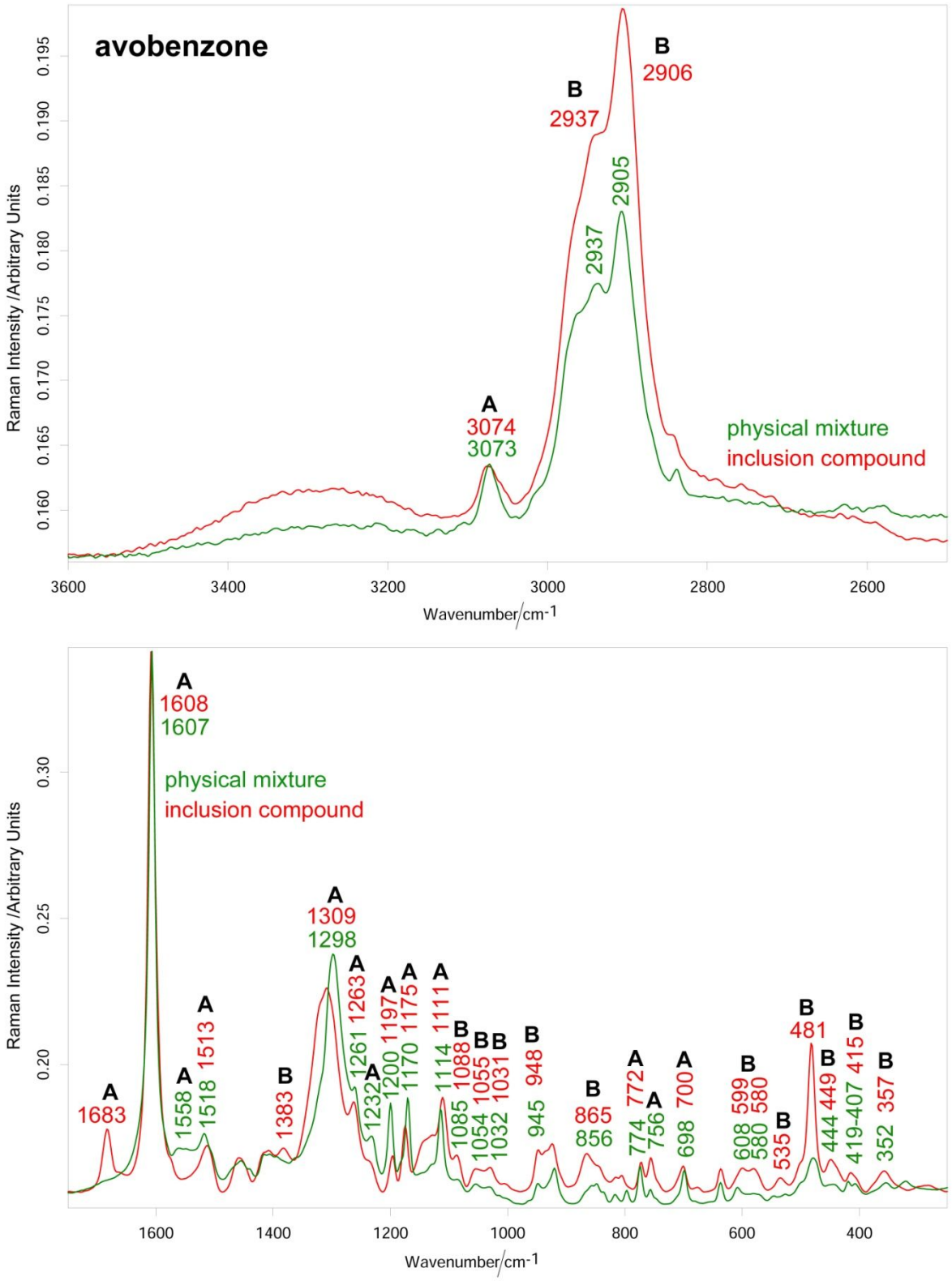

Figure SI-17. Raman spectra of $(\beta\text{-CD})_2\cdot A$ and 2:1 physical mixture. The main bands showing differences in the two spectra are indicated, and assigned prevalently to avobenzone (A) or β-CD (B).

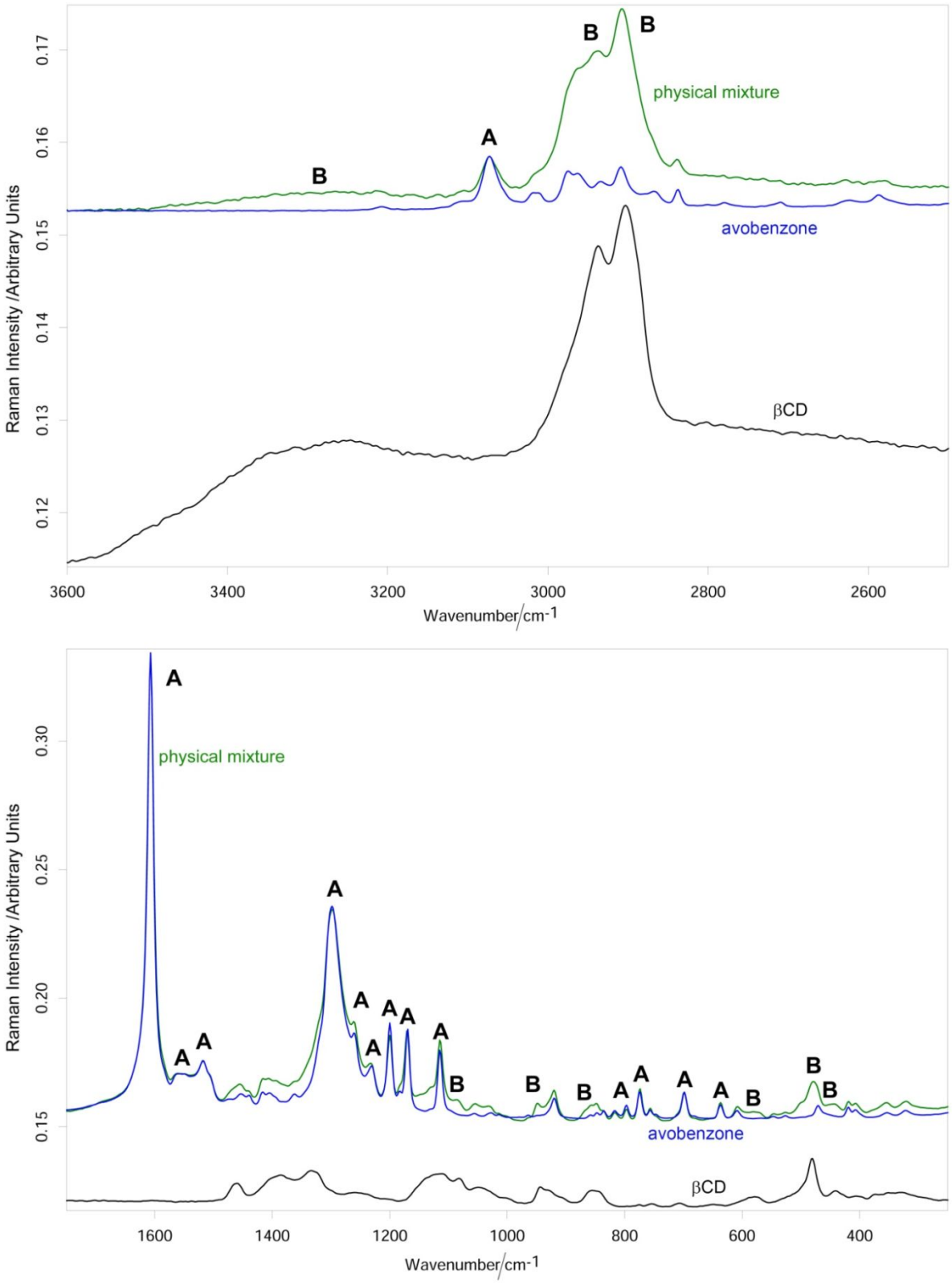

Figure SI-18. Raman spectrum of the 2:1 β-CD/avobenzone physical mixture. The spectra of avobenzone and β-CD are reported for comparison. The bands in the spectrum of the physical mixture prevalently assignable to avobenzone or β-CD are indicated with A and B, respectively. The bands not indicated have comparable contributions from both components.

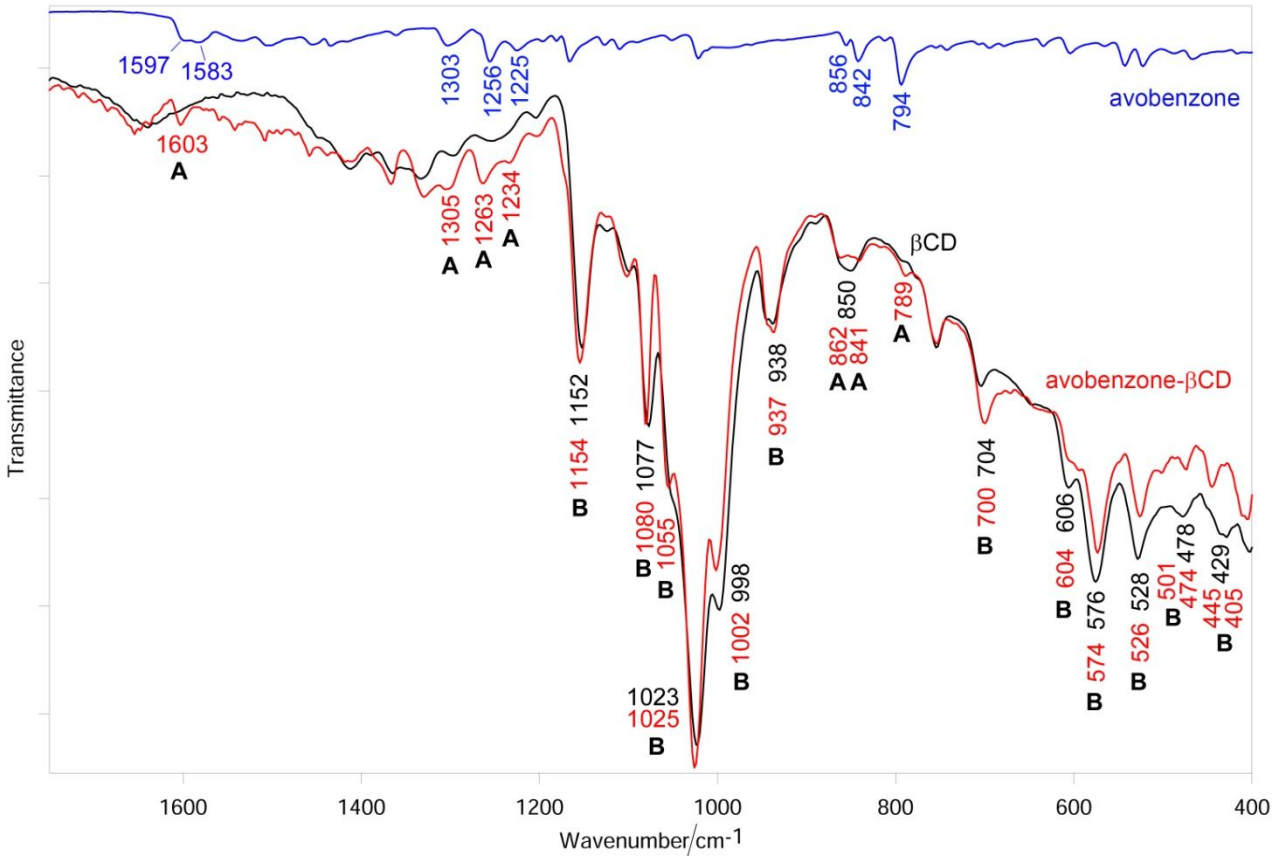

Figure SI-19. IR spectra of the $(\beta\text{-CD})_2\cdot A$, avobenzone and β-CD. The main bands of avobenzone and β-CD that underwent changes upon formation of the inclusion compound are indicated with A and B, respectively.

ESI-MS spectra

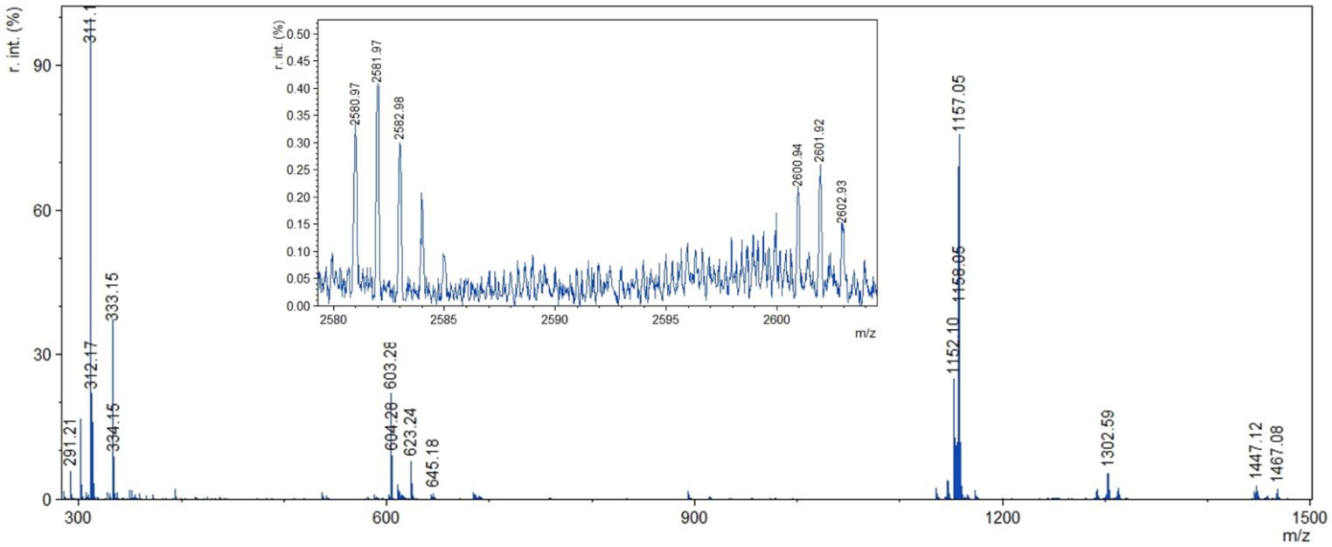

Figure SI-20. ESI-MS spectrum of the non-irradiated physical mixture containing the inclusion complexes $(\beta\text{-CD})_2\cdot$AVO and $(\beta\text{-CD})_3\cdot OCT_2$.

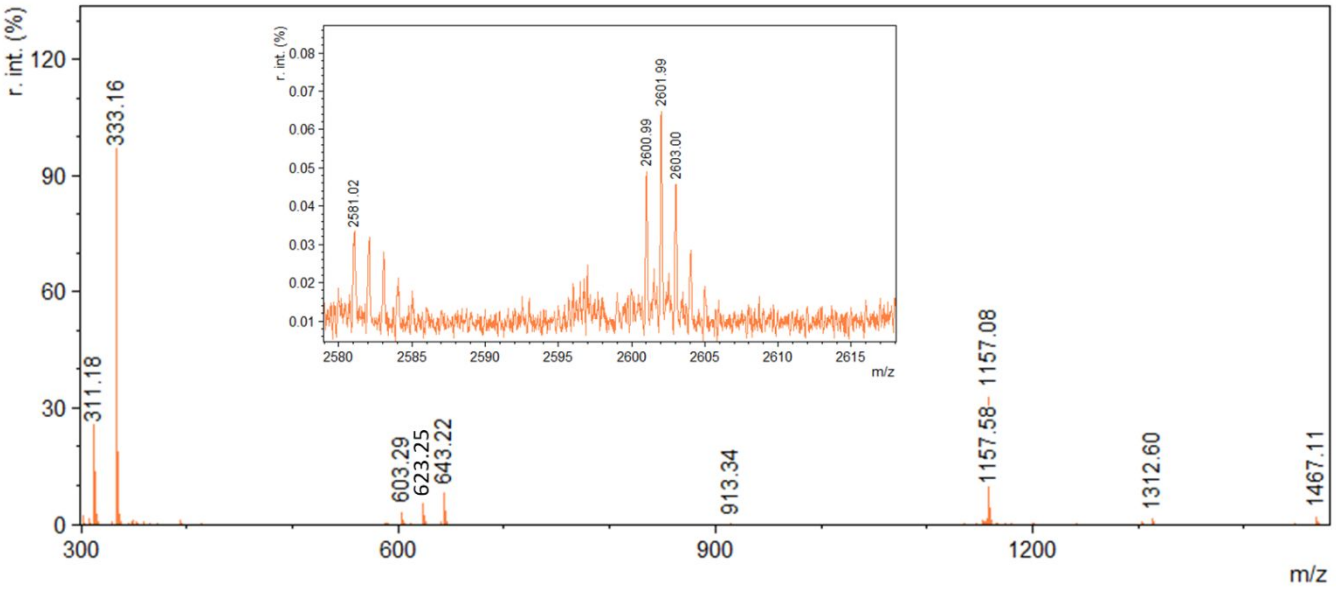

Figure SI-21. ESI-MS spectrum of the irradiated physical mixture containing the inclusion complexes $(\beta\text{-CD})_2\cdot$AVO and $(\beta\text{-CD})_3\cdot OCT_2$.

Table SI-4. List of the m/z peaks found in the ESI-MS spectrum solution of the non-irradiated inclusion complexes $(\beta\text{-CD})_2\cdot$AVO and $(\beta\text{-CD})_3\cdot OCT_2$.

m/z	int.	
291,2073	453,9766	$[OCT+H]^+$
311,1702	7698,495	$[AVO+H]^+$
313,182	1304,758	$[OCT+Na]^+$
333,1457	2933,152	$[AVO+Na]^+$
603,2771	1760,921	$[2OCT+Na]^+$
623,2391	620,4783	$[AVO+OCT+Na]^+$
643,2004	75,95998	$[2AVO+Na]^+$
1152,098	2018,459	$[\beta\text{-CD}+NH_4]^+$
1157,051	6170,942	$[\beta\text{-CD}+Na]^+$
1291,599	157,1981	$[OCT+2\beta\text{-CD}+H^++Na]^+$
1302,587	432,5796	$[OCT+2\ \beta\text{-CD}+2Na]^+$
1312,567	192,6248	$[AVO+2\ \beta\text{-CD}+2Na]^+$
1445,107	134,5882	$[AVO+\beta\text{-CD}+H]^+$
1447,115	221,2681	$[OCT+\beta\text{-CD}+Na]^+$
1467,078	171,3711	$[AVO+\beta\text{-CD}+Na]^+$
1724,491	716,0297	$[3\beta\text{-CD}+2Na]^+$
1869,52	194,877	
1879,503	139,8818	
2291,918	462,4195	
2581,97	31,8599	$[OCT+2\beta\text{-CD}+Na]^+$
2601,924	19,70599	$[AVO+2\beta\text{-CD}+Na]^+$

Here it can be evidenced the presence of different stoichiometries for the host guest system[10,11], as 1:1 H:G $[AVO+\ \beta\text{-CD}+H]^+$, $[OCT+\ \beta\text{-CD}+Na]^+$, $[AVO+\ \beta\text{-CD}+Na]^+$ at m/z 1445, 1447 and 1467, respectively. For the stoichiometry 2:1, doubly charged peaks, m/z 1302 and 1312 for species $[OCT+2\ \beta\text{-CD}+2Na]^{2+}$and $[AVO+2\ \beta\text{-CD}+2Na]^{2+}$, as well as singly charged species at very low intensity $[OCT+\ 2\ \beta\text{-CD}+Na]^+$ and $[AVO+2\ \beta\text{-CD}+Na]^+$ at m/z 2582 and 2602.

It must be noticed that octinoxate being less easily ionized, in this solvents system, with respect to avobenzone, results in a lower intensity of the mass peak. The spectrum of $(\beta\text{-CD})_2\cdot$AVO and $(\beta\text{-CD})_3\cdot OCT_2$ after irradiation was similar, as shown in SI-19.

Unexpected peaks were found in these spectra at around 600 m/z and more precisely at 603, 623 and 643. These peaks were expected to appear only after irradiation, due to the formation of molecular dimers via [2+2] photoinduced cyclization.[12] MS/MS for all three peaks was conducted and it results that at 603 m/z, by increasing collision energy, the peak at 313 appeared, after MS/MS at 623 the peaks at 313 and 333 appeared (Figure 5) and after MS/MS at 643 the peak at 333 appeared. This means that the peaks at higher m/z are an artefact of the analysis, ionizing two molecules together.

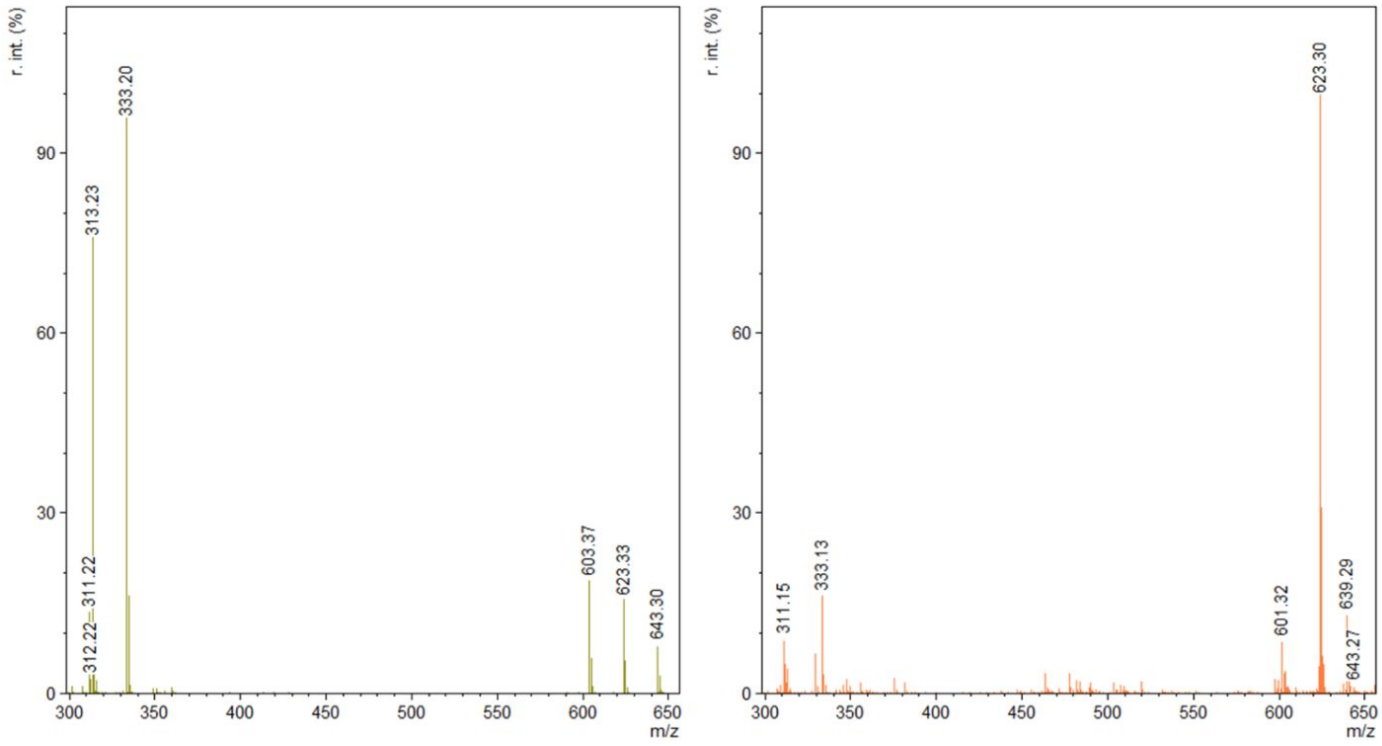

Figure SI-22. MS spectra for a mixture of avobenzone and octinoxate before (left) and after (right) UV irradiation. In the spectrum of the irradiated sample the peak revealing the photoadduct at 623 m/z ([2+2] photoreaction of AVO and OCTI) is predominant and also a small peak around 639 m/z, associated with the adduct $[AVO+OCT+K]^+$ is present here and could not be found before irradiation.

6eV

12eV

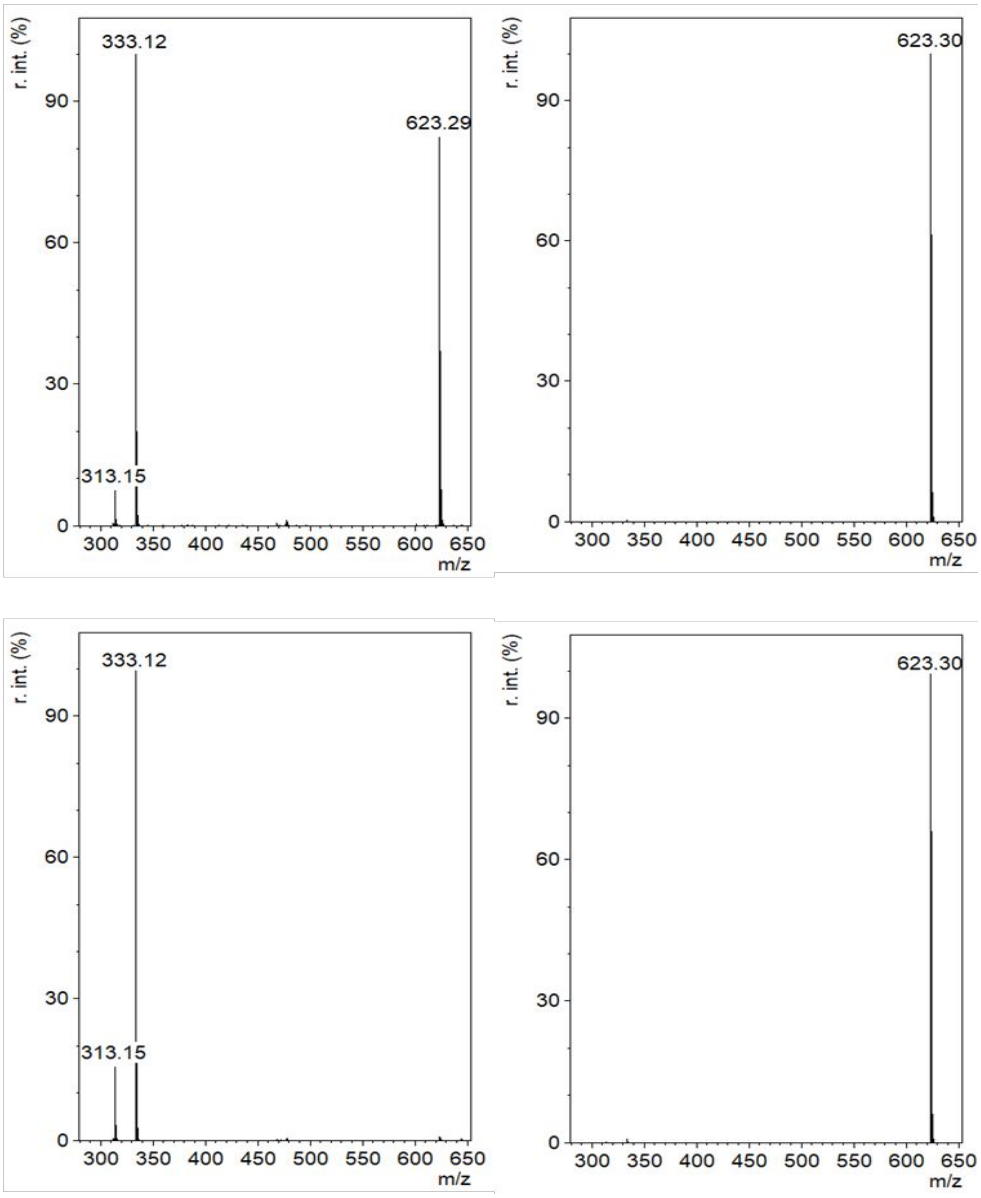

Figure SI-23. MS/MS spectra with collision energy at 6eV (top) and 12eV (bottom) of the peak at m/z 623 for: (left) a mixture of avobenzone and octinoxate, (right ~~middle~~) the same mixture after irradiation. Peak at 623 highlights the photodimerization product.

UV-VIS spectra

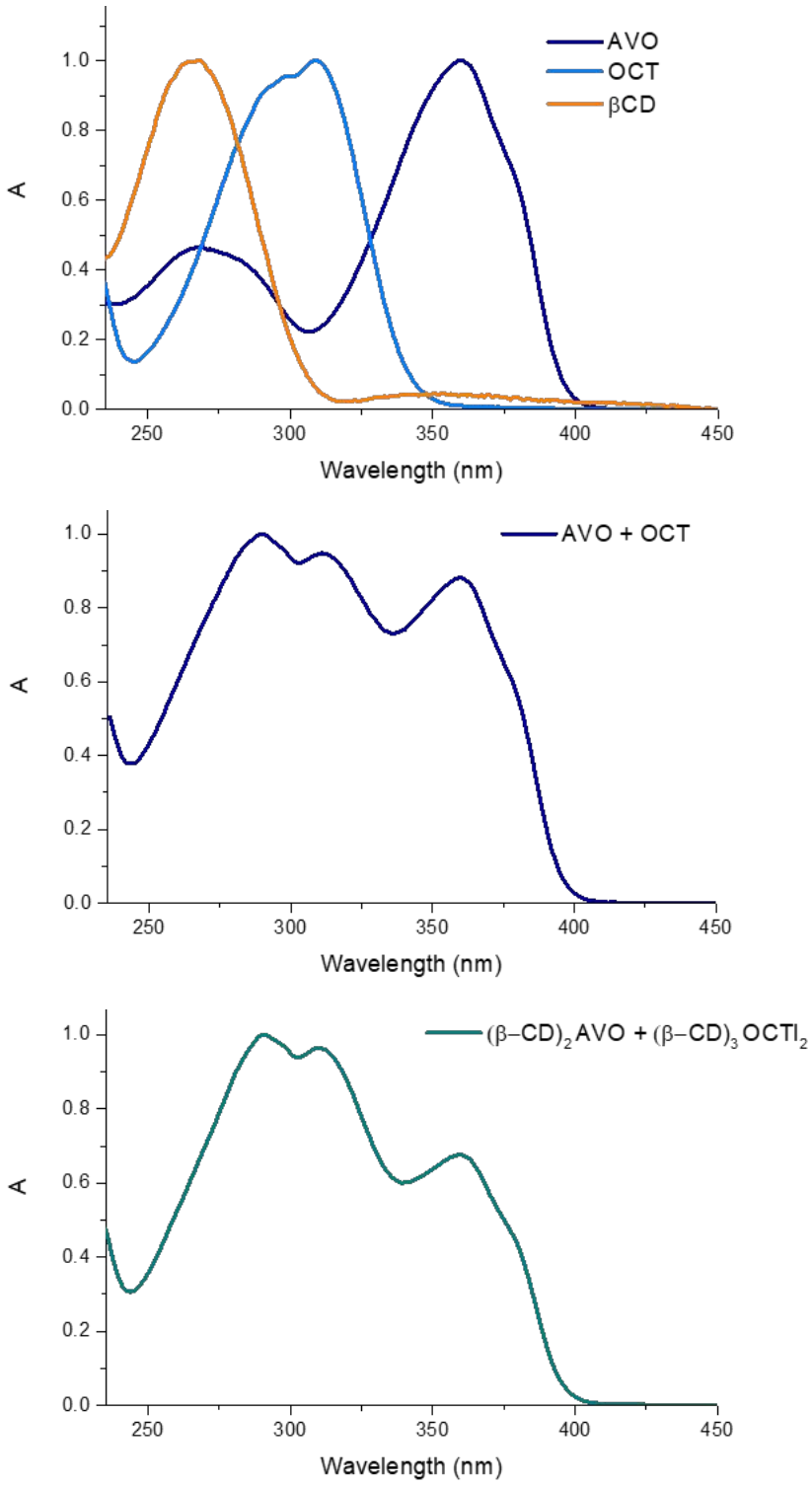

Figure SI-24. Normalized UV-VIS spectra of: (a) the three reactants used, (b) a solution containing equimolar amounts of the sunscreens, and (c) a solution containing an equimolar amount of $(\beta\text{-CD})_2\cdot$AVO, and $(\beta\text{-CD})_3\cdot OCT_2$. Note how the spectral features of the sunscreens remain unaltered after complexation.

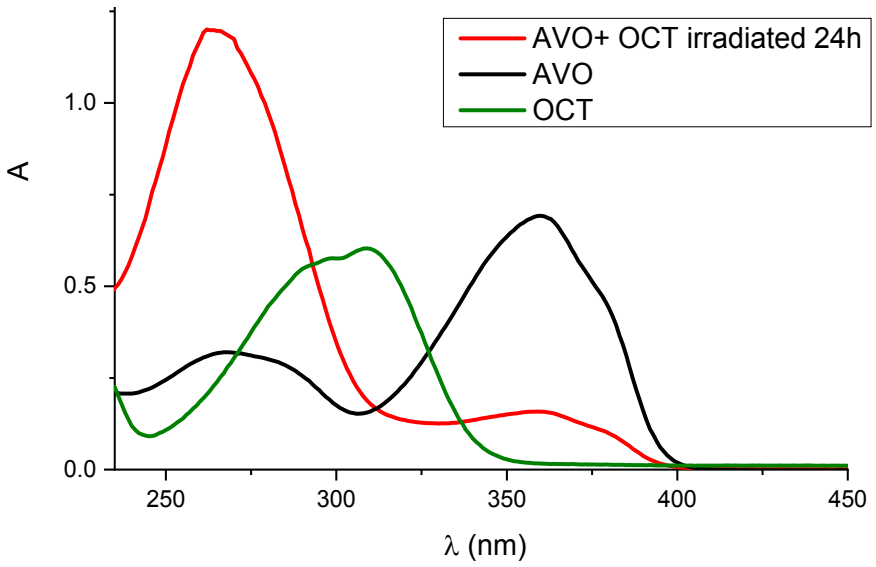

Figure SI-25. UV-VIS spectra recorded in a 50:50 water/ACN solution of avobenzone (black line), octinoxate (green line) and the mixture of the two irradiated for 24 hours (red line).

References

(1) Kagawa, H.; Sagawa, M.; Kakuta, A. 3-(4-tert-Butylphenyl)-3-hydroxy-1-(4-methoxyphenyl)-2-propen-1-one: An SHG Active B-diketone. *Acta Crystallogr. Sect. C* **1993**, *49* (12), 2181–2183. https://doi.org/10.1107/S0108270193005906.

(2) Divakar, S. Structure of a β-Cyclodextrin-Vanillin Inclusion Complex. *J. Agric. Food Chem.* **1990**, *38* (4), 940–944. https://doi.org/10.1021/jf00094a005.

(3) Beyere, L.; Yarasi, S.; Loppnow, G. R. Solvent Effects on Sunscreen Active Ingredients Using Raman Spectroscopy. *J. Raman Spectrosc.* **2003**, *34* (10), 743–750. https://doi.org/10.1002/jrs.1042.

(4) Russell, N. R.; McNamara, M. FT-IR and Raman Spectral Evidence for Metal Complex Formation with β-Cyclodextrin as a First Sphere Ligand. *J. Incl. Phenom. Mol. Recognit. Chem.* **1989**, *7* (4), 455–460. https://doi.org/10.1007/BF01079781.

(5) Costa, M. M. da; Alves, L. P.; Osório, R. A. L.; Pacheco, M. T. T.; Silveira, L. Detecting Active Ingredients of Insect Repellents and Sunscreens Topically in Skin by Raman Spectroscopy. *J. Biomed. Opt.* **2018**, *23* (10), 1. https://doi.org/10.1117/1.jbo.23.10.107003.

(6) Tayyari, S. F.; Rahemi, H.; Nekoei, A. R.; Zahedi-Tabrizi, M.; Wang, Y. A. Vibrational Assignment and Structure of Dibenzoylmethane. A Density Functional Theoretical Study. *Spectrochim. Acta - Part A Mol. Biomol. Spectrosc.* **2007**, *66* (2), 394–404. https://doi.org/10.1016/j.saa.2006.03.010.

(7) Hammond, G. S.; Borduin, W. G.; Guter, G. A. Chelates of β-Diketones. I. Enolization, Ionization and Spectra. *J. Am. Chem. Soc.* **1959**, *81* (17), 4682–4686. https://doi.org/10.1021/ja01526a058.

(8) Rachmawati, H.; Edityaningrum, C. A.; Mauludin, R. Molecular Inclusion Complex of Curcumin-β-Cyclodextrin Nanoparticle to Enhance Curcumin Skin Permeability from Hydrophilic Matrix Gel. *AAPS PharmSciTech* **2013**, *14* (4), 1303–1312. https://doi.org/10.1208/s12249-013-0023-5.

(9) Mohan, P. R. K.; Sreelakshmi, G.; Muraleedharan, C. V.; Joseph, R. Water Soluble Complexes of Curcumin with Cyclodextrins: Characterization by FT-Raman Spectroscopy. *Vib. Spectrosc.* **2012**, *62*, 77–84. https://doi.org/10.1016/j.vibspec.2012.05.002.

(10) Al-Burtomani, S. K. S.; Suliman, F. E. O. Inclusion Complexes of Norepinephrine with β-Cyclodextrin, 18-Crown-6 and Cucurbit[7]Uril: Experimental and Molecular Dynamics Study. *RSC Adv.* **2017**, *7* (16), 9888–9901. https://doi.org/10.1039/C6RA28638K.

(11) Suliman, F. E. O.; Varghese, B. Inclusion Complexes of Pantoprazole with β-Cyclodextrin and Cucurbit[7]Uril: Experimental and Molecular Modeling Study. *J. Incl. Phenom. Macrocycl. Chem.* **2018**, *91* (3–4), 179–188. https://doi:10.1007/s10847-018-0814-0.

(12) Dondi, D.; Albini, A.; Serpone, N. Interactions between Different Solar UVB/UVA Filters Contained in Commercial Suncreams and Consequent Loss of UV Protection. *Photochem. Photobiol. Sci.* **2006**, *5* (9), 835–843. https://doi: 10.1039/b606768a.